

Quantum Geometry Probed by Chiral Excitonic Optical Response of Chern Insulators

Wen-Xuan Qiu¹ and Fengcheng Wu^{1,2,*}

¹*School of Physics and Technology, Wuhan University, Wuhan 430072, China*

²*Wuhan Institute of Quantum Technology, Wuhan 430206, China*

We theoretically derive the sum rule for the negative first moment of the absorptive optical conductivity with excitonic effects and establish its connection to the quantum weight K and Chern number C of the ground state. Applying this framework, we investigate the excitonic optical response of the Chern insulator at hole filling factor $\nu = 1$ in twisted bilayer MoTe₂. A single chiral exciton state, which selectively absorbs circularly polarized light of a specific handedness, dominates the optical sum rule. The chiral exciton state comprises two types of interlayer electron-hole transitions, which cancel out the total out-of-plane dipole moment. The absorption spectrum shows nearly perfect magnetic circular dichroism, which can be attributed to the nearly saturated bound $K \geq |C|$ of the Chern insulator under study. Our work illustrates the potential of using excitonic optical responses to probe quantum geometry encoded by K and C .

Introduction.—The quantum geometric tensor of Bloch states consists of Berry curvature and quantum metric, which characterize, respectively, the phase and amplitude distances between nearby quantum states [1]. Quantum geometry, by capturing the structure of Bloch wavefunctions [2, 3], plays an important role in charge transport [4–15], optical responses [16–23], and many-body physics [24–33]. For an insulator, the integral of the Berry curvature over the Brillouin zone gives the Chern number C , which is a well-known topological invariant that measures the Hall conductivity in a unit of e^2/h [4]. This Chern number C also governs magnetic circular dichroism (MCD) via a sum rule for the optical Hall conductivity [34]. By comparison, the Brillouin-zone integral of the quantum metric trace has been identified as the quantum weight K , which lacks topological invariance but is observable, as it is proportional to the first negative moment of longitudinal optical conductivity [34–36]. The impact of the quantum geometry on optical responses has resulted in a topological bound on band gap and a prediction of perfect MCD when the trace inequality $K \geq |C|$ is saturated [34, 37]. Numerical investigations have explored these phenomena in systems of twisted bilayer MoTe₂ (t MoTe₂) [34, 37] and MnBi₂Te₄ thin films [38]. On the other hand, optical responses are often subjected to excitonic effects due to electron-hole interactions, which were not taken into account in the previous studies [34, 37, 38]. The relationship between the quantum geometry of the ground state and the excitonic optical response is a fundamental problem that remains to fully be explored.

In this Letter, we derive the sum rule for the negative first moment of the absorptive optical conductivity, incorporating excitonic effects. A connection between this sum rule and the ground-state quantum geometric quantities K and C is established. As an illustrative example, we investigate the Chern insulator (CI), also known as the quantum anomalous Hall insulator, in t MoTe₂ at

$\nu = 1$ [39–43]. By solving the Bethe-Salpeter equation, we calculate the exciton states of this system. The optical spectrum exhibits pronounced excitonic effects, featuring a single dominant chiral exciton state. We numerically validate the derived optical sum rule and find a significant contribution from the exciton state. We further elucidate that while optical sum rules can bound the optical gap, they do not constrain the charge gap. Additionally, we conduct a comparative investigation of the optical spectrum in a topologically trivial state. Our study underscores the important role of quantum geometry in constraining excitonic optical response and lays a foundation for optically probing the quantum geometry.

Optical sum rules.— We calculate the optical conductivity $\sigma_{\alpha\beta}$ for an insulator as a function of frequency ω at zero temperature by Kubo formula,

$$\sigma_{\alpha\beta}(\omega) = i \frac{e^2}{\hbar} \frac{1}{\mathcal{A}} \sum_{\chi} \frac{1}{\mathcal{E}_{\chi}} \left[\frac{V_{G\chi}^{\alpha} V_{\chi G}^{\beta}}{\hbar\omega - \mathcal{E}_{\chi} + i\eta} + \frac{V_{\chi G}^{\alpha} V_{G\chi}^{\beta}}{\hbar\omega + \mathcal{E}_{\chi} + i\eta} \right], \quad (1)$$

where e is the elementary charge, \mathcal{A} is the system size, $V_{\chi G}^{\alpha} = \langle \chi | \hat{v}^{\alpha} | G \rangle$ is the optical matrix element with velocity operator $\hat{v} = i[\hat{\mathcal{H}}, \hat{r}]$ along direction α . Here \hat{r} is the position operator of a many-body system [see definition in Eq. (3)], $\hat{\mathcal{H}}$ is the Hamiltonian, $|G\rangle$ is the ground state, \mathcal{E}_{χ} is the energy of an excited state $|\chi\rangle$ measured relative to that of $|G\rangle$, and $\eta \rightarrow 0^+$. We focus on two-dimensional systems with an out-of-plane threefold rotational symmetry \hat{C}_{3z} , where $\sigma_{xx} = \sigma_{yy}$ and $\sigma_{xy} = -\sigma_{yx}$. The absorptive part of optical conductivity can then be defined as $\sigma_{\alpha\beta}^{\text{abs}} = \delta_{\alpha\beta} \text{Re}\sigma_{\alpha\beta} + i(1 - \delta_{\alpha\beta}) \text{Im}\sigma_{\alpha\beta}$. The negative first moment $W_{\alpha\beta}^{(1)}$ of $\sigma_{\alpha\beta}^{\text{abs}}$ is calculated to be,

$$\begin{aligned} W_{\alpha\beta}^{(1)} &= \int_0^{\infty} d\omega \frac{\sigma_{\alpha\beta}^{\text{abs}}(\omega)}{\omega} = \frac{e^2}{\hbar} \frac{\pi}{\mathcal{A}} \sum_{\chi} w_{\alpha\beta}^{(1)}(\chi) \\ &= \frac{e^2}{\hbar} \frac{\pi}{\mathcal{A}} [\langle \hat{r}^{\alpha} \hat{r}^{\beta} \rangle_G - \langle \hat{r}^{\alpha} \rangle_G \langle \hat{r}^{\beta} \rangle_G], \end{aligned} \quad (2)$$

where $w_{\alpha\beta}^{(1)}(\chi) = V_{G\chi}^{\alpha} V_{\chi G}^{\beta} / \mathcal{E}_{\chi}^2$ and $\langle \dots \rangle_G$ represents the ground state expectation value. Equation (2) connects

* wufcheng@whu.edu.cn

the generalized optical weight $W_{\alpha\beta}^{(1)}$ with the mean-square fluctuation of polarization in the ground state [35]. $W_{\alpha\beta}^{(1)}$ can be further expressed using the quantum geometric quantities of the many-body ground state under twisted boundary conditions [34, 35].

To avoid the complexity involved in the twisted boundary condition while making analytical progress, we focus on the special yet widely applicable case where $|G\rangle$ can be approximated by a Slater determinant composed of occupied Bloch states $|o\mathbf{k}\rangle$. Here o is the band index and \mathbf{k} labels momentum. The unoccupied Bloch states are denoted as $|\bar{o}\mathbf{k}\rangle$. In the complete Bloch basis, the position operator \hat{r} in the second quantized form is [23, 44],

$$\begin{aligned}\hat{r} &= \sum_{\mathbf{k}} \sum_{mn} r_{mn}(\mathbf{k}) f_{\mathbf{k},m}^\dagger f_{\mathbf{k},n}, \\ r_{mn}(\mathbf{k}) &= \delta_{mn} i\partial_{\mathbf{k}} - \mathbf{A}_{mn}(\mathbf{k}), \\ \mathbf{A}_{mn}(\mathbf{k}) &= -\langle u_{m\mathbf{k}} | i\partial_{\mathbf{k}} | u_{n\mathbf{k}} \rangle,\end{aligned}\quad (3)$$

where $|u_{n\mathbf{k}}\rangle$ is the periodic part of the Bloch state $|n\mathbf{k}\rangle$ and $\mathbf{A}_{mn}(\mathbf{k})$ is the Berry connection. We take Eq. (3) as the operative definition of \hat{r} . $W_{\alpha\beta}^{(1)}$ can then be expressed as,

$$W_{\alpha\beta}^{(1)} = \frac{e^2}{\hbar} \frac{\pi}{\mathcal{A}} \sum_{\mathbf{k}} \sum_{\bar{o}o} A_{\bar{o}o}^\alpha(\mathbf{k}) A_{\bar{o}o}^\beta(\mathbf{k}) = \frac{e^2}{\hbar} \frac{\pi}{\mathcal{A}} \sum_{\mathbf{k}} \text{Tr} \mathcal{Q}^{\alpha\beta}(\mathbf{k}), \quad (4)$$

where $\mathcal{Q}_{\bar{o}o'}^{\alpha\beta} = \sum_{\bar{o}} A_{\bar{o}o}^\alpha A_{\bar{o}o'}^\beta$ is the quantum geometric tensor of occupied bands [3] and $(\mathcal{Q}^{\alpha\beta})^\dagger = \mathcal{Q}^{\beta\alpha}$. The symmetric and antisymmetric parts of $\mathcal{Q}^{\alpha\beta}$ concerning the spatial indices define, respectively, the non-Abelian quantum metric and Berry curvature, $\mathcal{Q}^{\alpha\beta} = G^{\alpha\beta} + \frac{i}{2}\epsilon^{\alpha\beta}\Omega$, where $\epsilon^{\alpha\beta}$ is the antisymmetric tensor. The real and imaginary parts of Eq. (4) are,

$$\int_0^\infty d\omega \frac{\text{Re}[\sigma_{\alpha\alpha}(\omega)]}{\omega} = \frac{\pi}{2} \frac{e^2}{\hbar} K, \quad \alpha = x \text{ or } y, \quad (5)$$

$$\int_0^\infty d\omega \frac{\text{Im}[\sigma_{\alpha\beta}(\omega)]}{\omega} = \frac{\pi}{2} \frac{e^2}{\hbar} \epsilon^{\alpha\beta} C, \quad \alpha \neq \beta, \quad (6)$$

where $K = \frac{1}{2\pi} \sum_{\alpha} \int d^2\mathbf{k} \text{Tr} G^{\alpha\alpha}$ is identified as the quantum weight [34] and $C = \frac{1}{2\pi} \int d^2\mathbf{k} \text{Tr} \Omega$ is the Chern number. Here the approximation of $|G\rangle$ being a Slater determinant is used, but no such approximation is required for the excited states $|\chi\rangle$. Since $|\chi\rangle$ can be exciton states induced by electron-hole attraction, Eqs. (5) and (6) establish generalized sum rules for excitonic optical response in terms of quantum geometric quantities of ground state. In the noninteracting case, Eq. (4) reduces to the sum rule obtained in Ref. 34.

The optical conductivity in response to circularly polarized light is $\sigma_{\pm} = \sigma_{xx} \pm i\sigma_{xy}$, of which the absorptive part is,

$$\text{Re}\sigma_{\pm}(\omega) = \text{Re}\sigma_{xx}(\omega) \mp \text{Im}\sigma_{xy}(\omega). \quad (7)$$

The inequality $\text{Re}\sigma_{\pm}(\omega) \geq 0$ implies that $K \geq |C|$, which can be proved since the 2×2 matrix Λ with $\Lambda_{\alpha\beta} = \text{Tr} \mathcal{Q}^{\alpha\beta}$ is semipositive definite. When the bound is saturated ($K = |C|$), either $\text{Re}\sigma_{+}(\omega)$ or $\text{Re}\sigma_{-}(\omega)$ is strictly zero (depending on the sign of C), which leads to perfect MCD.

Excitonic optical response. — We use the CI in $t\text{MoTe}_2$ at hole filling factor $\nu = 1$, which has been experimentally realized [39–43], as an example to demonstrate the connection between excitonic optical response and quantum geometry. In our calculation, we use a band-projected interacting model by retaining the top eight moiré valence bands in $t\text{MoTe}_2$. The moiré bands are obtained by solving the continuum model [45] with the parameters from Ref. [46]. Since we study holes doped into the system, we construct the projected Hamiltonian $\hat{\mathcal{H}}$ in the hole basis, which includes both the single-particle term $\hat{\mathcal{H}}_0$ and the Coulomb interaction term $\hat{\mathcal{H}}_{\text{int}}$,

$$\begin{aligned}\hat{\mathcal{H}}_0 &= \sum_{\mathbf{k},\tau,n} \mathcal{E}_{\mathbf{k}}^{n\tau} b_{\mathbf{k}n\tau}^\dagger b_{\mathbf{k}n\tau}, \\ \hat{\mathcal{H}}_{\text{int}} &= \frac{1}{2} \sum V_{\mathbf{k}_1\mathbf{k}_2\mathbf{k}_3\mathbf{k}_4}^{n_1n_2n_3n_4}(\tau,\tau') b_{\mathbf{k}_1n_1\tau}^\dagger b_{\mathbf{k}_2n_2\tau'}^\dagger b_{\mathbf{k}_3n_3\tau'} b_{\mathbf{k}_4n_4\tau}.\end{aligned}\quad (8)$$

Here $b_{\mathbf{k}n\tau}^\dagger$ ($b_{\mathbf{k}n\tau}$) is the hole creation (annihilation) operator for the n th moiré valence band at momentum \mathbf{k} and valley τ . Here $\tau = +(-)$ is equivalent to spin up (down) [45]. $\mathcal{E}_{\mathbf{k}}^{n\tau}$ accounts for the single-particle band energy and $V_{\mathbf{k}_1\mathbf{k}_2\mathbf{k}_3\mathbf{k}_4}^{n_1n_2n_3n_4}(\tau,\tau')$ is the Coulomb potential $V_{\mathbf{q}} = 2\pi e^2 \tanh(|\mathbf{q}|d)/(\epsilon|\mathbf{q}|)$ projected onto the moiré bands, where d is the gate-to-sample distance and ϵ is the dielectric constant. In our calculation, we set $d = 20$ nm, $\epsilon = 20$ (See Supplemental Material [47] for numerical details).

We perform mean-field studies of $\hat{\mathcal{H}}$ using self-consistent Hartree-Fock (HF) approximation at $\nu = 1$. We find two types of ground states separated by a first-order phase transition and tuned by the twist angle θ of $t\text{MoTe}_2$: (1) the CI phase with valley polarization but no layer polarization for $3.15^\circ < \theta < 5.0^\circ$ and (2) the phase with both layer polarization and valley polarization (LP-VP phase) for $2.0^\circ < \theta < 3.15^\circ$. This phase diagram is consistent with previous studies [48, 49]

The mean-field Hamiltonian for both the CI and LP-FM_z phases can be formally written as

$$\hat{\mathcal{H}}_{\text{MF}} = \sum_{\mathbf{k},\tau,\lambda} E_{\mathbf{k}}^{\lambda\tau} f_{\mathbf{k}\lambda\tau}^\dagger f_{\mathbf{k}\lambda\tau}, \quad (9)$$

where $E_{\mathbf{k}}^{\lambda\tau}$ includes the band energy and HF self energy. Here $f_{\mathbf{k}\lambda\tau}^\dagger$ and $b_{\mathbf{k}n\tau}^\dagger$ operators are related by unitary transformations, $f_{\mathbf{k}\lambda\tau}^\dagger = \sum_n U_{n\lambda}^{k\tau} b_{\mathbf{k}n\tau}^\dagger$. In Fig. 1(a) [Fig. 2(a)], we show the mean-field band structure for the CI (LP-VP) phase, where the occupied band in the hole basis is layer hybridized (layer polarized) and carries a Chern number C of $|C| = 1(0)$. For definiteness, the occupied band is assumed to be polarized to $\tau = +$ valley in the following.

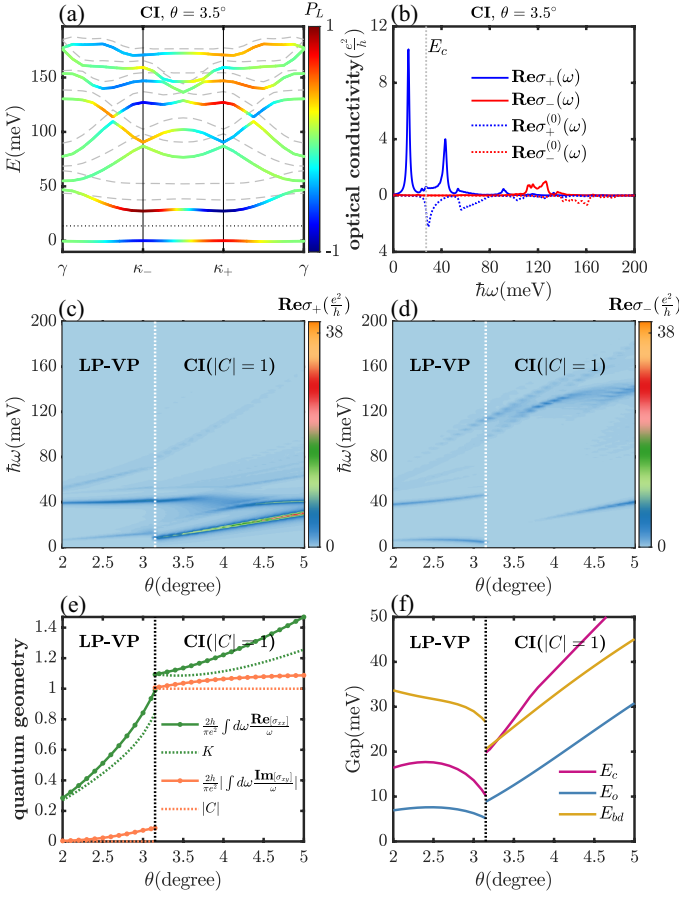


FIG. 1. (a) HF band structure of CI state at $\theta = 3.5^\circ$ in the hole basis. The solid (long dashed) lines plot bands in $\tau = +(-)$ valley. The dotted line marks the middle of the gap. The color represents the layer polarization P_L with $+1$ (-1) indicating the bottom (top) layer. (b) $\text{Re}\sigma_{\pm}(\omega)$ for the CI state in (a). $\text{Re}\sigma_{\pm}^{(0)}(\omega)$ is calculated without electron-hole interaction. The vertical dotted line marks the minimum direct gap E_c . (c), (d) $\text{Re}\sigma_{\pm}(\omega)$ as a function of θ and $\hbar\omega$. White dotted lines separate the LP-VP and CI phases. (e) Quantum geometry obtained through optical sum rules (solid lines) and ground state (dashed lines). (f) The minimum direct gap E_c (pink line), the optical gap E_o (blue line), and the bound E_{bd} (yellow line) as functions of θ .

We now study intravalley excited states with zero center-of-mass momentum, which can be optically probed. In the presence of electron-hole interactions, the excited states can be parametrized as [50]

$$|\chi\rangle = \sum_{\mathbf{k}, \lambda \geq 2} z_{\mathbf{k}, \lambda}(\chi) f_{\mathbf{k}\lambda+}^{\dagger} f_{\mathbf{k}1+} |G\rangle, \quad (10)$$

where $|G\rangle$ is the Slater-determinant ground state obtained in the HF approximation. Variation of the energy $\langle \chi | \mathcal{H} | \chi \rangle$ with respect to the parameter $z_{\mathbf{k}, \lambda}(\chi)$ leads to

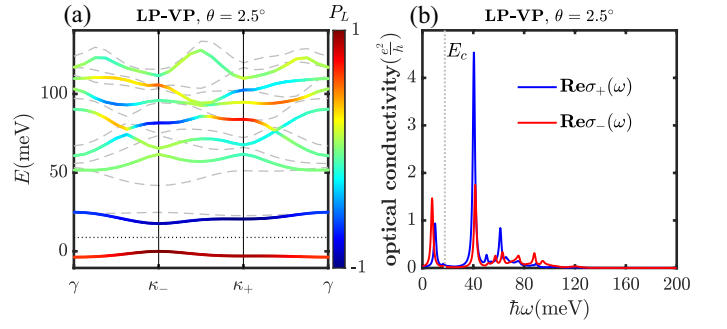


FIG. 2. (a) HF band structure of LP-VP state at $\theta = 2.5^\circ$. (b) $\text{Re}\sigma_{\pm}(\omega)$ for the LP-VP state in (a).

the Bethe-Salpeter (BS) equation,

$$\mathcal{E}_{\chi} z_{\mathbf{k}, \lambda}(\chi) = \sum_{\mathbf{p}, \lambda'} \mathcal{H}_{\mathbf{k}\mathbf{p}}^{\lambda\lambda'} z_{\mathbf{p}, \lambda'}(\chi), \quad (11)$$

$$\mathcal{H}_{\mathbf{k}\mathbf{p}}^{\lambda\lambda'} = (E_{\mathbf{k}}^{\lambda+} - E_{\mathbf{k}}^{\lambda+}) \delta_{\mathbf{k}\mathbf{p}} \delta_{\lambda\lambda'} - (\tilde{V}_{\mathbf{p}\mathbf{k}\mathbf{p}\mathbf{k}}^{1\lambda\lambda'1} - \tilde{V}_{\mathbf{k}\mathbf{p}\mathbf{p}\mathbf{k}}^{\lambda\lambda'1}),$$

where $\mathcal{H}_{\mathbf{k}\mathbf{p}}^{\lambda\lambda'}$ includes the quasiparticle energy cost of particle-hole transition as well as direct and exchange two-particle matrix element. Here \tilde{V} denotes Coulomb matrix element in the basis of $f_{\mathbf{k}\lambda+}^{\dagger}$ operators.

We solve the BS equation to obtain $|\chi\rangle$ and \mathcal{E}_{χ} , which are used to calculate the optical conductivity in Eq. (1). An optically active state, as an eigenstate of the \hat{C}_{3z} symmetry, responds exclusively to either left or right circularly polarized light and therefore, is chiral. Because time-reversal symmetry is spontaneously broken by the valley polarization, excited states with opposite chiralities are energetically nondegenerate, but both types can be present in the spectrum. The calculated absorption spectrum $\text{Re}\sigma_{\pm}(\omega)$ for the CI phase at $\theta = 3.5^\circ$, shown in Fig. 1(b), has two noticeable features: (1) the spectrum exhibits nearly perfect MCD with vanishing $\text{Re}\sigma_{-}$ for $\hbar\omega$ up to 110meV; (2) the spectrum is dominated by a large chiral excitonic peak in $\text{Re}\sigma_{+}$ at an energy E_o below E_c , where E_o represents the optical gap and E_c is the minimum direct gap in the HF band structure. In comparison, we also calculate the spectrum $\text{Re}\sigma_{\pm}^{(0)}(\omega)$ without including the electron-hole interactions, where the response is smeared out over energies above E_c [Fig. 1(b)]. The dependence of $\text{Re}\sigma_{\pm}(\omega)$ on θ is shown in Figs. 1(c) and 1(d), where the above two features are generic for the CI phase.

The CI phase should always have a finite MCD because of the sum rule for the Hall conductivity in Eq. (6) and the finite Chern number C . On the other hand, the nearly perfect MCD observed above is a special property of $t\text{MoTe}_2$, where K and $|C|$ in the QAHE phase almost saturate the bound $K \geq |C|$ as shown in Fig. 1(e). The deviation measured by $(K - |C|)/(K + |C|)$ is as low as 4% at $\theta = 3.5^\circ$, explaining the nearly vanishing $\text{Re}\sigma_{-}$ (here $C = -1$). We note that $K = |C|$ is identified as the ideal trace condition which can favor fractionalized

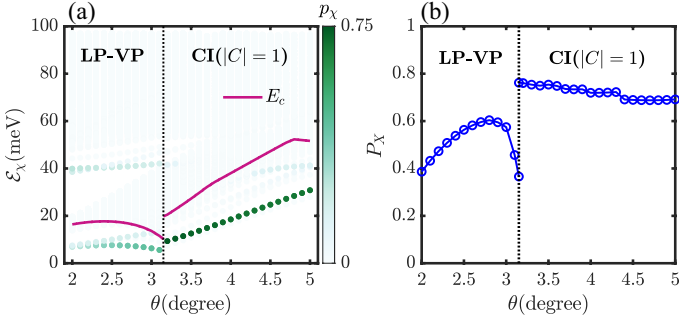


FIG. 3. (a) The color encodes p_χ for each excited state. The purple line marks E_c . (b) P_X as a function of θ .

states [27]. By contrast, the LP-VP phase has $C = 0$ and should have weak MCD according to Eq. (6). This is indeed the case as shown by the absorption spectrum in Fig. 2(b) for the LP-VP phase, where $\text{Re}\sigma_-$ and $\text{Re}\sigma_+$ do not show a strong contrast.

We compare values of $W_{\alpha\beta}^{(1)}$ calculated using, respectively, the excited states based on Eq. (2) and the quantum geometry of ground state based on Eq. (4). The results obtained from the two approaches are not identical but have a semi-quantitative agreement, as plotted in Fig. 1(e). The discrepancy comes from the fact that $|\mathcal{G}\rangle$ and $|\chi\rangle$ used in our calculation are only approximate but not exact eigenstates of the interacting Hamiltonian $\hat{\mathcal{H}}$, while the sum rules are derived in the eigenbasis of $\hat{\mathcal{H}}$.

The exciton states can contribute significantly to $W_{\alpha\beta}^{(1)}$ because they have low energies and large optical matrix elements. To quantify the contribution of each excited state to $W_{xx}^{(1)}$, we define $p_\chi = \frac{w_{xx}^{(1)}(\chi)}{\sum_{\chi'} w_{xx}^{(1)}(\chi')}$. As shown in Fig. 3(a), the exciton states can have a sizable p_χ . For example, the single dominating chiral exciton at $\theta = 3.5^\circ$ in the CI phase has $p_\chi = 0.73$. We further define $P_X = \sum_{\varepsilon_\chi < E_c} p_\chi$ to count the contribution of all exciton states below E_c , which can reach up to 0.8 (0.6) in the CI (LP-VP) phase [Fig. 3(b)].

An upper bound E_{bd} can be put on the optical gap E_o (the lowest energy of optically active excitons) by comparing Eq. (5) with the f sum rule given by

$$\int_0^\infty d\omega \text{Re}\sigma_{xx}(\omega) = \frac{\pi n_c e^2}{2m^*}, \quad (12)$$

where m^* is the effective mass and n_c is the carrier density. The bound E_{bd} is $\frac{2\pi\hbar^2 n_c}{m^* K}$. Our numerical results indeed satisfy the bound $E_o < E_{bd}$, as shown in Fig. 1(f). However, we emphasize that E_c , which would be the optical gap if electron-hole interactions were neglected, is not bounded by E_{bd} [Fig. 1(f)].

Exciton wave function.— We examine the character of the dominating chiral exciton in the CI phase, which consists of particle-hole transitions in the $\tau = +$ valley mainly from the first band ($\lambda = 1$) to the second band ($\lambda = 2$). The momentum-space wavefunction $|z_{\mathbf{k},2}\rangle$ of

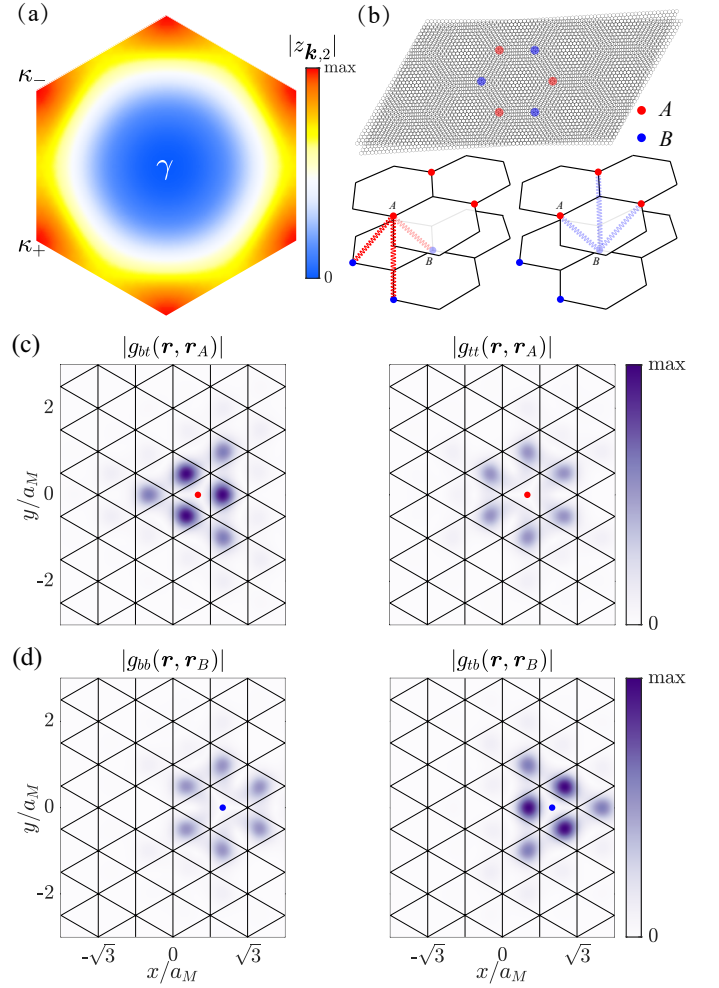


FIG. 4. Wavefunction of the dominating exciton in the CI phase at $\theta = 3.5^\circ$. (a) $|z_{\mathbf{k},2}\rangle$ in the moiré Brillouin zone. (b) Top panel: Moiré superlattices of $t\text{MoTe}_2$ with A and B sites. Bottom panel: schematic illustration of interlayer excitations. (c), (d) $|g_{ll'}(\mathbf{r}, \mathbf{r}')|$ plotted in \mathbf{r} space for different l with fixed \mathbf{r}' and l' . a_M is the moiré period.

this exciton at $\theta = 3.5^\circ$ is shown in Fig. 4(a), which exhibits two peaks at the moiré Brillouin zone corners κ_+ and κ_- . Around κ_+ , the first and second bands are polarized, respectively, to the bottom (b) and top (t) layers of $t\text{MoTe}_2$, as illustrated in Fig. 1(a). The situation is opposite around κ_- , where the first (second) band is polarized to the t (b) layer. Therefore, the exciton comprises interlayer particle-hole transitions but has zero out-of-plane dipole moment due to the superposition of excitations at κ_+ and κ_- . The real-space exciton wavefunction $g_{ll'}(\mathbf{r}, \mathbf{r}')$ also exhibits interesting patterns, where l (l') is the layer index and \mathbf{r} (\mathbf{r}') is the in-plane position of the p^* (h^*) particle. Here p^* (h^*) labels the particle (hole) in the hole basis that we employ. Low-energy carriers in the t and b layer of $t\text{MoTe}_2$ are, respectively, confined to A and B sites in the moiré superlattice, which form a buckled honeycomb lattice [Fig. 4(b)]. When h^* is fixed

in the t layer at an A site with position \mathbf{r}_A , the wavefunction $g_{tA}(\mathbf{r}, \mathbf{r}_A)$ is peaked at three nearest-neighbor B sites in the b layer, as plotted in Fig. 4(c). Figure 4(d) shows a similar pattern for $g_{tB}(\mathbf{r}, \mathbf{r}_B)$.

Discussion.— In summary, we present a theory that connects the quantum geometry of the ground state with the excitonic optical response through the optical sum rules. We illustrate the implication of the quantum geometry on the excitonic optical response using the CI states in $t\text{MoTe}_2$ as an example and demonstrate that exciton states can dominate the optical sum rule. This dominant contribution makes it practical to probe the quantum weight K and Chern number C using only the low-energy optical spectrum based on Eqs. (5) and (6). We note that the Chern number C can be independently measured by the Hall conductivity through current transport. Therefore, the quantum weight K can be determined through the ratio K/C , which only requires relative values of $\text{Re}\sigma_{\pm}(\omega)$. It is particularly interesting to

examine how close the bound $K \geq |C|$ is saturated, as the saturated bound $K = |C|$ signals the resemblance of a Chern band and the lowest Landau level [27, 51]. As we show in $t\text{MoTe}_2$, the relevant optical response of CI states is typically in the infrared or terahertz frequency range, which can be experimentally probed using available techniques [52–54]. Extending beyond $t\text{MoTe}_2$, we anticipate that the quantum geometry can be explored through excitonic optical response across a diverse range of systems.

Acknowledgments.— We thank Lingjie Du and Yanhao Tang for valuable discussions. This work is supported by National Key Research and Development Program of China (Grants No. 2021YFA1401300 and No. 2022YFA1402401), National Natural Science Foundation of China (Grant No. 12274333). W.-X. Q. is also supported by the China Postdoctoral Science Foundation (Grant No. 2023M742716). The numerical calculations in this paper have been done on the supercomputing system in the Supercomputing Center of Wuhan University.

-
- [1] P. Törmä, Essay: Where can quantum geometry lead us?, *Phys. Rev. Lett.* **131**, 240001 (2023).
- [2] J. P. Provost and G. Vallee, Riemannian structure on manifolds of quantum states, *Commun. Math. Phys.* **76**, 289 (1980).
- [3] Y.-Q. Ma, S. Chen, H. Fan, and W.-M. Liu, Abelian and non-abelian quantum geometric tensor, *Phys. Rev. B* **81**, 245129 (2010).
- [4] D. J. Thouless, M. Kohmoto, M. P. Nightingale, and M. den Nijs, Quantized hall conductance in a two-dimensional periodic potential, *Phys. Rev. Lett.* **49**, 405 (1982).
- [5] Q. Niu, D. J. Thouless, and Y.-S. Wu, Quantized hall conductance as a topological invariant, *Phys. Rev. B* **31**, 3372 (1985).
- [6] F. D. M. Haldane, Model for a Quantum Hall Effect without Landau Levels: Condensed-Matter Realization of the “Parity Anomaly”, *Phys. Rev. Lett.* **61**, 2015 (1988).
- [7] D. Vanderbilt, *Berry Phases in Electronic Structure Theory: Electric Polarization, Orbital Magnetization and Topological Insulators* (Cambridge University Press, 2018).
- [8] Y. Gao, S. A. Yang, and Q. Niu, Field induced positional shift of bloch electrons and its dynamical implications, *Phys. Rev. Lett.* **112**, 166601 (2014).
- [9] I. Sodemann and L. Fu, Quantum nonlinear hall effect induced by berry curvature dipole in time-reversal invariant materials, *Phys. Rev. Lett.* **115**, 216806 (2015).
- [10] Q. Ma, S.-Y. Xu, H. Shen, D. MacNeill, V. Fatemi, T.-R. Chang, A. M. Mier Valdivia, S. Wu, Z. Du, C.-H. Hsu, S. Fang, Q. D. Gibson, K. Watanabe, T. Taniguchi, R. J. Cava, E. Kaxiras, H.-Z. Lu, H. Lin, L. Fu, N. Gedik, and P. Jarillo-Herrero, Observation of the nonlinear hall effect under time-reversal-symmetric conditions, *Nature* **565**, 337 (2019).
- [11] C. Wang, Y. Gao, and D. Xiao, Intrinsic Nonlinear Hall Effect in Antiferromagnetic Tetragonal CuMnAs , *Phys. Rev. Lett.* **127**, 277201 (2021).
- [12] K. Das, S. Lahiri, R. B. Atencia, D. Culcer, and A. Agarwal, Intrinsic nonlinear conductivities induced by the quantum metric, *Phys. Rev. B* **108**, L201405 (2023).
- [13] D. Kaplan, T. Holder, and B. Yan, Unification of Nonlinear Anomalous Hall Effect and Nonreciprocal Magnetoresistance in Metals by the Quantum Geometry, *Phys. Rev. Lett.* **132**, 026301 (2024).
- [14] A. Gao, Y.-F. Liu, J.-X. Qiu, B. Ghosh, T. V. Trevisan, Y. Onishi, C. Hu, T. Qian, H.-J. Tien, S.-W. Chen, M. Huang, D. Bérubé, H. Li, C. Tzschaschel, T. Dinh, Z. Sun, S.-C. Ho, S.-W. Lien, B. Singh, K. Watanabe, T. Taniguchi, D. C. Bell, H. Lin, T.-R. Chang, C. R. Du, A. Bansil, L. Fu, N. Ni, P. P. Orth, Q. Ma, and S.-Y. Xu, Quantum metric nonlinear Hall effect in a topological antiferromagnetic heterostructure, *Science* **381**, 181 (2023).
- [15] N. Wang, D. Kaplan, Z. Zhang, T. Holder, N. Cao, A. Wang, X. Zhou, F. Zhou, Z. Jiang, C. Zhang, S. Ru, H. Cai, K. Watanabe, T. Taniguchi, B. Yan, and W. Gao, Quantum-metric-induced nonlinear transport in a topological antiferromagnet, *Nature* **621**, 487 (2023).
- [16] A. M. Cook, B. M. Fregoso, F. de Juan, S. Coh, and J. E. Moore, Design principles for shift current photovoltaics, *Nat. Commun* **8**, 14176 (2017).
- [17] F. de Juan, A. G. Grushin, T. Morimoto, and J. E. Moore, Quantized circular photogalvanic effect in weyl semimetals, *Nat. Commun* **8**, 15995 (2017).
- [18] J. Ahn, G.-Y. Guo, and N. Nagaosa, Low-frequency divergence and quantum geometry of the bulk photovoltaic effect in topological semimetals, *Phys. Rev. X* **10**, 041041 (2020).
- [19] T. Holder, D. Kaplan, and B. Yan, Consequences of time-reversal-symmetry breaking in the light-matter interaction: Berry curvature, quantum metric, and diabatic motion, *Phys. Rev. Res.* **2**, 033100 (2020).
- [20] P. Bhalla, K. Das, D. Culcer, and A. Agarwal, Resonant second-harmonic generation as a probe of quantum geometry, *Phys. Rev. Lett.* **129**, 227401 (2022).

- [21] C. Aversa and J. E. Sipe, Nonlinear optical susceptibilities of semiconductors: Results with a length-gauge analysis, *Phys. Rev. B* **52**, 14636 (1995).
- [22] J. Orenstein, J. Moore, T. Morimoto, D. Torchinsky, J. Harter, and D. Hsieh, Topology and symmetry of quantum materials via nonlinear optical responses, *ANNU REV CONDEN MA P* **12**, 247 (2021).
- [23] J. Ahn, G.-Y. Guo, N. Nagaosa, and A. Vishwanath, Riemannian geometry of resonant optical responses, *Nat. Phys* **18**, 290 (2022).
- [24] R. Roy, Band geometry of fractional topological insulators, *Phys. Rev. B* **90**, 165139 (2014).
- [25] S. Peotta and P. Törmä, Superfluidity in topologically nontrivial flat bands, *Nat. Commun* **6**, 8944 (2015).
- [26] P. J. Ledwith, G. Tarnopolsky, E. Khalaf, and A. Vishwanath, Fractional chern insulator states in twisted bilayer graphene: An analytical approach, *Phys. Rev. Res.* **2**, 023237 (2020).
- [27] J. Wang, J. Cano, A. J. Millis, Z. Liu, and B. Yang, Exact Landau level description of geometry and interaction in a flatband, *Phys. Rev. Lett.* **127**, 246403 (2021).
- [28] P. Törmä, S. Peotta, and B. A. Bernevig, Superconductivity, superfluidity and quantum geometry in twisted multilayer systems, *Nat. Rev. Phys* **4**, 528 (2022).
- [29] H. Tian, X. Gao, Y. Zhang, S. Che, T. Xu, P. Cheung, K. Watanabe, T. Taniguchi, M. Randeria, F. Zhang, C. N. Lau, and M. W. Bockrath, Evidence for Dirac flat band superconductivity enabled by quantum geometry, *Nature* **614**, 440 (2023).
- [30] J. Yu, C. J. Ciccarino, R. Bianco, I. Errea, P. Narang, and B. A. Bernevig, Non-trivial quantum geometry and the strength of electron-phonon coupling, *Nat. Phys* [10.1038/s41567-024-02486-0](https://doi.org/10.1038/s41567-024-02486-0) (2024).
- [31] A. Srivastava and A. Imamoglu, Signatures of Bloch-band geometry on excitons: Nonhydrogenic spectra in transition-metal dichalcogenides, *Phys. Rev. Lett.* **115**, 166802 (2015).
- [32] F. Wu and S. Das Sarma, Quantum geometry and stability of moiré flatband ferromagnetism, *Phys. Rev. B* **102**, 165118 (2020).
- [33] H.-Y. Xie, P. Ghaemi, M. Mitranò, and B. Uchoa, Theory of topological exciton insulators and condensates in flat Chern bands, [arXiv:2311.04970](https://arxiv.org/abs/2311.04970).
- [34] Y. Onishi and L. Fu, Fundamental bound on topological gap, *Phys. Rev. X* **14**, 0111052 (2024).
- [35] I. Souza, T. Wilkens, and R. M. Martin, Polarization and localization in insulators: Generating function approach, *Phys. Rev. B* **62**, 1666 (2000).
- [36] Y. Onishi and L. Fu, Quantum weight, [arXiv:2401.13847](https://arxiv.org/abs/2401.13847).
- [37] J. Dong, J. Wang, P. J. Ledwith, A. Vishwanath, and D. E. Parker, Composite Fermi Liquid at Zero Magnetic Field in Twisted MoTe₂, *Phys. Rev. Lett.* **131**, 136502 (2023).
- [38] B. Ghosh, Y. Onishi, S.-Y. Xu, H. Lin, L. Fu, and A. Bansil, Probing quantum geometry through optical conductivity and magnetic circular dichroism, [arXiv:2401.09689](https://arxiv.org/abs/2401.09689).
- [39] E. Anderson, F.-R. Fan, J. Cai, W. Holtzmann, T. Taniguchi, K. Watanabe, D. Xiao, W. Yao, and X. Xu, Programming correlated magnetic states with gate-controlled moiré geometry, *Science* **381**, 325 (2023).
- [40] J. Cai, E. Anderson, C. Wang, X. Zhang, X. Liu, W. Holtzmann, Y. Zhang, F. Fan, T. Taniguchi, K. Watanabe, Y. Ran, T. Cao, L. Fu, D. Xiao, W. Yao, and X. Xu, Signatures of fractional quantum anomalous Hall states in twisted MoTe₂, *Nature* **622**, 63 (2023).
- [41] Y. Zeng, Z. Xia, K. Kang, J. Zhu, P. Knüppel, C. Vaswani, K. Watanabe, T. Taniguchi, K. F. Mak, and J. Shan, Thermodynamic evidence of fractional Chern insulator in moiré MoTe₂, *Nature* **622**, 69 (2023).
- [42] H. Park, J. Cai, E. Anderson, Y. Zhang, J. Zhu, X. Liu, C. Wang, W. Holtzmann, C. Hu, Z. Liu, T. Taniguchi, K. Watanabe, J.-H. Chu, T. Cao, L. Fu, W. Yao, C.-Z. Chang, D. Cobden, D. Xiao, and X. Xu, Observation of fractionally quantized anomalous Hall effect, *Nature* **622**, 74 (2023).
- [43] F. Xu, Z. Sun, T. Jia, C. Liu, C. Xu, C. Li, Y. Gu, K. Watanabe, T. Taniguchi, B. Tong, J. Jia, Z. Shi, S. Jiang, Y. Zhang, X. Liu, and T. Li, Observation of Integer and Fractional Quantum Anomalous Hall Effects in Twisted Bilayer MoTe₂, *Phys. Rev. X* **13**, 031037 (2023).
- [44] R. Karplus and J. M. Luttinger, Hall effect in ferromagnetics, *Phys. Rev.* **95**, 1154 (1954).
- [45] F. Wu, T. Lovorn, E. Tutuc, I. Martin, and A. H. MacDonald, Topological Insulators in Twisted Transition Metal Dichalcogenide Homobilayers, *Phys. Rev. Lett.* **122**, 086402 (2019).
- [46] C. Wang, X.-W. Zhang, X. Liu, Y. He, X. Xu, Y. Ran, T. Cao, and D. Xiao, Fractional Chern Insulator in Twisted Bilayer MoTe₂, *Phys. Rev. Lett.* **132**, 036501 (2024).
- [47] See Supplemental Material at [url] for details on theoretical derivations and numerical calculations, which includes Refs. [55, 56].
- [48] W.-X. Qiu, B. Li, X.-J. Luo, and F. Wu, Interaction-Driven Topological Phase Diagram of Twisted Bilayer MoTe₂, *Phys. Rev. X* **13**, 041026 (2023).
- [49] B. Li, W.-X. Qiu, and F. Wu, Electrically tuned topology and magnetism in twisted bilayer MoTe₂ at $\nu_h = 1$, *Phys. Rev. B* **109**, L041106 (2024).
- [50] F. Wu, F. Qu, and A. H. MacDonald, Exciton band structure of monolayer MoS₂, *Phys. Rev. B* **91**, 075310 (2015).
- [51] B. Li and F. Wu, Variational Mapping of Chern Bands to Landau Levels: Application to Fractional Chern Insulators in Twisted MoTe₂, [arXiv:2405.20307](https://arxiv.org/abs/2405.20307).
- [52] L. Ju, L. Wang, T. Cao, T. Taniguchi, K. Watanabe, S. G. Louie, F. Rana, J. Park, J. Hone, F. Wang, and P. L. McEuen, Tunable excitons in bilayer graphene, *Science* **358**, 907 (2017).
- [53] Y. D. Kato, Y. Okamura, M. Hirschberger, Y. Tokura, and Y. Takahashi, Topological magneto-optical effect from skyrmion lattice, *Nat. Commun* **14**, 5416 (2023).
- [54] J. Liang, Z. Liu, Z. Yang, Y. Huang, U. Wurstbauer, C. R. Dean, K. W. West, L. N. Pfeiffer, L. Du, and A. Pinczuk, Evidence for chiral graviton modes in fractional quantum hall liquids, *Nature* **628**, 78 (2024).
- [55] X. Liu, Y. He, C. Wang, X.-W. Zhang, T. Cao, and D. Xiao, Gate-tunable antiferromagnetic Chern insulator in twisted bilayer transition metal dichalcogenides, *Phys. Rev. Lett.* **132**, 146401 (2024).
- [56] F.-R. Fan, C. Xiao, and W. Yao, Orbital Chern insulator at $\nu = -2$ in twisted MoTe₂, *Phys. Rev. B* **109**, L041403 (2024).

Supplemental Materials for “Quantum Geometry Probed by Chiral Excitonic Optical Response of Chern Insulators”

I. DETAILED DERIVATION OF THE GENERALIZED OPTICAL SUM RULE

The Kubo formula of Eq. (1) in the main text is given by,

$$\begin{aligned}\sigma_{\alpha\beta}(\omega) &= \sum_{\chi} F_{+}(\chi) V_{G\chi}^{\alpha} V_{\chi G}^{\beta} + F_{-}(\chi) V_{\chi G}^{\alpha} V_{G\chi}^{\beta}, \\ F_{\pm}(\chi) &= i \frac{e^2}{\hbar} \frac{1}{\mathcal{A}} \frac{1}{\mathcal{E}_{\chi}} \frac{1}{\hbar\omega \mp \mathcal{E}_{\chi} + i\eta}.\end{aligned}\tag{S1}$$

In the general case, the absorptive part of optical conductivity can be defined as [34],

$$\sigma_{\alpha\beta}^{\text{abs}}(\omega) = \text{Re}\sigma_{\alpha\beta}^L(\omega) + i \text{Im}\sigma_{\alpha\beta}^H(\omega), \quad \sigma_{\alpha\beta}^L(\omega) = \frac{\sigma_{\alpha\beta}(\omega) + \sigma_{\beta\alpha}(\omega)}{2}, \quad \sigma_{\alpha\beta}^H(\omega) = \frac{\sigma_{\alpha\beta}(\omega) - \sigma_{\beta\alpha}(\omega)}{2}.\tag{S2}$$

From Eq (S1), we obtain

$$\sigma_{\alpha\beta}^L(\omega) = \sum_{\chi} [F_{+}(\chi) + F_{-}(\chi)] \text{Re}[V_{G\chi}^{\alpha} V_{\chi G}^{\beta}], \quad \sigma_{\alpha\beta}^H(\omega) = \sum_{\chi} i[F_{+}(\chi) - F_{-}(\chi)] \text{Im}[V_{G\chi}^{\alpha} V_{\chi G}^{\beta}],\tag{S3}$$

and

$$\sigma_{\alpha\beta}^{\text{abs}}(\omega) = \sum_{\chi} V_{G\chi}^{\alpha} V_{\chi G}^{\beta} \text{Re}F_{+}(\chi) + (V_{G\chi}^{\alpha} V_{\chi G}^{\beta})^* \text{Re}F_{-}(\chi).\tag{S4}$$

Using $\lim_{\eta \rightarrow 0^+} \frac{1}{x+i\eta} = P\left(\frac{1}{x}\right) - i\pi\delta(x)$,

$$\text{Re}F_{\pm}(\chi) = \frac{e^2}{\hbar} \frac{\pi}{\mathcal{A}} \frac{1}{\mathcal{E}_{\chi}} \delta(\hbar\omega \mp \mathcal{E}_{\chi}).\tag{S5}$$

Therefore, the negative first moment $W_{\alpha\beta}^{(1)}$ of $\sigma_{\alpha\beta}^{\text{abs}}(\omega)$ is calculated to be,

$$W_{\alpha\beta}^{(1)} = \int_0^{\infty} d\omega \frac{\sigma_{\alpha\beta}^{\text{abs}}(\omega)}{\omega} = \frac{e^2}{\hbar} \frac{\pi}{\mathcal{A}} \sum_{\chi} w_{\alpha\beta}^{(1)}(\chi),\tag{S6}$$

where $w_{\alpha\beta}^{(1)}(\chi) = V_{G\chi}^{\alpha} V_{\chi G}^{\beta} / \mathcal{E}_{\chi}^2$. By incorporating $\hat{v} = i[\hat{\mathcal{H}}, \hat{\mathbf{r}}]$ into $V_{G\chi}^{\alpha} = \langle G | \hat{v}^{\alpha} | \chi \rangle$ and $V_{\chi G}^{\beta} = \langle \chi | \hat{v}^{\beta} | G \rangle$,

$$\sum_{\chi} w_{\alpha\beta}^{(1)}(\chi) = \sum_{\chi} \frac{\langle G | \hat{r}^{\alpha} \hat{\mathcal{H}} - \hat{\mathcal{H}} \hat{r}^{\alpha} | \chi \rangle \langle \chi | \hat{\mathcal{H}} \hat{r}^{\beta} - \hat{r}^{\beta} \hat{\mathcal{H}} | G \rangle}{\mathcal{E}_{\chi}^2} = \sum_{\chi} \langle G | \hat{r}^{\alpha} | \chi \rangle \langle \chi | \hat{r}^{\beta} | G \rangle = \langle G | \hat{r}^{\alpha} \hat{r}^{\beta} | G \rangle - \langle G | \hat{r}^{\alpha} | G \rangle \langle G | \hat{r}^{\beta} | G \rangle.\tag{S7}$$

We focus on the special case where $|G\rangle$ can be approximated by a Slater determinant composed of occupied Bloch states $|o\mathbf{k}\rangle$. Here o is the band index and \mathbf{k} labels momentum. The unoccupied Bloch states are denoted as $|\bar{o}\mathbf{k}\rangle$. In the complete basis of $\{|o\mathbf{k}\rangle, |\bar{o}\mathbf{k}\rangle\}$, the position operator $\hat{\mathbf{r}}$ in the second quantized form is expressed as [23, 44],

$$\hat{\mathbf{r}}(\mathbf{k}) = \sum_{\mathbf{k}} \sum_{mn} \mathbf{r}_{mn}(\mathbf{k}) f_{\mathbf{k},m}^{\dagger} f_{\mathbf{k},n}, \quad \mathbf{r}_{mn}(\mathbf{k}) = \delta_{mn} i\partial_{\mathbf{k}} - \mathbf{A}_{mn}(\mathbf{k}), \quad \mathbf{A}_{mn}(\mathbf{k}) = -\langle u_{m\mathbf{k}} | i\partial_{\mathbf{k}} | u_{n\mathbf{k}} \rangle,\tag{S8}$$

where $|u_{n\mathbf{k}}\rangle$ is the periodic part of the Bloch state $|n\mathbf{k}\rangle$ and $\mathbf{A}_{mn}(\mathbf{k})$ is the Berry connection. Then

$$\begin{aligned}\langle G | \hat{r}^{\alpha} \hat{r}^{\beta} | G \rangle &= \sum_{\mathbf{k}_1} \sum_{m_1 n_1} \sum_{\mathbf{k}_2} \sum_{m_2 n_2} r_{m_1 n_1}^{\alpha}(\mathbf{k}_1) r_{m_2 n_2}^{\beta}(\mathbf{k}_2) \langle G | f_{\mathbf{k}_1, m_1}^{\dagger} f_{\mathbf{k}_1, n_1} f_{\mathbf{k}_2, m_2}^{\dagger} f_{\mathbf{k}_2, n_2} | G \rangle \\ &= \sum_{\mathbf{k}_1 \mathbf{k}_2} \sum_{o_1 o_2} r_{o_1 o_1}^{\alpha}(\mathbf{k}_1) r_{o_2 o_2}^{\beta}(\mathbf{k}_2) + \sum_{\mathbf{k}} \sum_{o\bar{o}} r_{o\bar{o}}^{\alpha}(\mathbf{k}) r_{\bar{o}o}^{\beta}(\mathbf{k}), \\ \langle G | \hat{r}^{\alpha} | G \rangle \langle G | \hat{r}^{\beta} | G \rangle &= \sum_{\mathbf{k}_1 \mathbf{k}_2} \sum_{o_1 o_2} r_{o_1 o_1}^{\alpha}(\mathbf{k}_1) r_{o_2 o_2}^{\beta}(\mathbf{k}_2).\end{aligned}\tag{S9}$$

By combining Eqs. (S7), (S8) and (S9), Eq. (S6) can be further written as,

$$W_{\alpha\beta}^{(1)} = \frac{e^2}{\hbar} \frac{\pi}{\mathcal{A}} \sum_{\mathbf{k}} \sum_{o\bar{o}} r_{o\bar{o}}^\alpha(\mathbf{k}) r_{o\bar{o}}^\beta(\mathbf{k}) = \frac{e^2}{\hbar} \frac{\pi}{\mathcal{A}} \sum_{\mathbf{k}} \sum_{o\bar{o}} A_{o\bar{o}}^\alpha(\mathbf{k}) A_{o\bar{o}}^\beta(\mathbf{k}) = \frac{e^2}{\hbar} \frac{\pi}{\mathcal{A}} \sum_{\mathbf{k}} \text{Tr} \mathcal{Q}^{\alpha\beta}, \quad (\text{S10})$$

where $\mathcal{Q}_{o\bar{o}o'}^{\alpha\beta} = \sum_{\bar{o}} A_{o\bar{o}}^\alpha A_{\bar{o}o'}^\beta$ is the quantum geometric tensor of occupied bands [3].

To study the response to circularly polarized light, we define the velocity operator $\hat{v}^\pm = \frac{1}{\sqrt{2}} (\hat{v}^x \pm i\hat{v}^y)$ and the optical matrix element $V_{\chi G}^\pm = \langle \chi | \hat{v}^\pm | G \rangle$. The corresponding optical conductivity is given by,

$$\begin{aligned} \sigma_\pm(\omega) &= i \frac{e^2}{\hbar} \frac{1}{\mathcal{A}} \sum_{\chi} \frac{1}{\mathcal{E}_\chi} \left[\frac{V_{G\chi}^\mp V_{\chi G}^\pm}{\hbar\omega - \mathcal{E}_\chi + i\eta} + \frac{V_{\chi G}^\mp V_{G\chi}^\pm}{\hbar\omega + \mathcal{E}_\chi + i\eta} \right] \\ &= i \frac{e^2}{2\hbar} \frac{1}{\mathcal{A}} \sum_{\chi} \frac{1}{\mathcal{E}_\chi} \left[\frac{\left(V_{G\chi}^x V_{\chi G}^x + V_{G\chi}^y V_{\chi G}^y \pm i V_{G\chi}^x V_{\chi G}^y \mp i V_{G\chi}^y V_{\chi G}^x \right)}{\hbar\omega - \mathcal{E}_\chi + i\eta} + \frac{\left(V_{\chi G}^x V_{G\chi}^x + V_{\chi G}^y V_{G\chi}^y \pm i V_{\chi G}^x V_{G\chi}^y \mp i V_{\chi G}^y V_{G\chi}^x \right)}{\hbar\omega + \mathcal{E}_\chi + i\eta} \right] \\ &= \frac{1}{2} [\sigma_{xx}(\omega) + \sigma_{yy}(\omega) \pm i\sigma_{xy}(\omega) \mp i\sigma_{yx}(\omega)]. \end{aligned} \quad (\text{S11})$$

We focus on two-dimensional systems with an out-of-plane threefold rotational symmetry \hat{C}_{3z} , where $\sigma_{xx} = \sigma_{yy}$ and $\sigma_{xy} = -\sigma_{yx}$, which leads to Eq. (7) in the main text.

II. MODEL HAMILTONIAN AND GROUND STATE CALCULATIONS

A. Moiré Hamiltonian

Moiré superlattices of $t\text{MoTe}_2$ respect a threefold rotation \hat{C}_{3z} around the out-of-plane \hat{z} axis and a twofold rotation \hat{C}_{2y} around the in-plane \hat{y} axis that exchanges the bottom (b) and top (t) layers. The single-particle moiré Hamiltonian of $t\text{MoTe}_2$ has been constructed in Ref. [45] for valence band states in $\pm K$ valley as,

$$\begin{aligned} \hat{\mathcal{H}}_0^\tau &= \begin{pmatrix} -\frac{\hbar^2(\hat{\mathbf{k}} - \tau\boldsymbol{\kappa}_+)^2}{2m^*} + \Delta_+(\mathbf{r}) & \Delta_{T,\tau}(\mathbf{r}) \\ \Delta_{T,\tau}^\dagger(\mathbf{r}) & -\frac{\hbar^2(\hat{\mathbf{k}} - \tau\boldsymbol{\kappa}_-)^2}{2m^*} + \Delta_-(\mathbf{r}) \end{pmatrix}, \\ \Delta_\pm(\mathbf{r}) &= 2V \sum_{j=1,3,5} \cos(\mathbf{g}_j \cdot \mathbf{r} \pm \psi), \\ \Delta_{T,\tau}(\mathbf{r}) &= w (1 + e^{-i\tau\mathbf{g}_2 \cdot \mathbf{r}} + e^{-i\tau\mathbf{g}_3 \cdot \mathbf{r}}), \end{aligned} \quad (\text{S12})$$

where the 2×2 Hamiltonia $\hat{\mathcal{H}}_0^\tau$ is expressed in the layer-pseudospin space. The index $\tau = \pm$ labels $\pm K$ valleys, which are also locked to spin \uparrow and \downarrow , respectively. $\Delta_\pm(\mathbf{r})$ is the layer-dependent potential with an amplitude V and phase parameters $\pm\psi$, and $\Delta_{T,\tau}(\mathbf{r})$ is the interlayer tunneling with a strength w . \mathbf{r} and $\hat{\mathbf{k}} = -i\partial_{\mathbf{r}}$ are respectively, the position and momentum operators. m^* is the effective mass. $\boldsymbol{\kappa}_\pm = [4\pi/(3a_M)](-\sqrt{3}/2, \mp 1/2)$ are located at corners of the moiré Brillouin zone, and $\mathbf{g}_j = [4\pi/(\sqrt{3}a_M)]\{\cos[(j-1)\pi/3], \sin[(j-1)\pi/3]\}$ for $j = 1, \dots, 6$ are the moiré reciprocal lattice vectors, where $a_M \approx a_0/\theta$ is the moiré period and a_0 is the monolayer lattice constant.

In this work, we focus on the Chern insulator (CI) phase for θ around 3.5° , where the Bloch states have a nearly ideal quantum geometry. For this range of θ , appropriate parameters can be taken as, $a_0 = 3.52\text{\AA}$, $m^* = 0.6m_e$, $V = 20.8\text{ meV}$, $\psi = -107.7^\circ$, $w = -23.8\text{ meV}$, as used in Refs. [46, 55, 56], where m_e is the electron bare mass.

B. Band-projected Interacting Hamiltonian

The moiré Hamiltonian $\hat{\mathcal{H}}_0^\tau$ in Eq. (S12) can be solved within plane wave basis to obtain the energy $\varepsilon_{\mathbf{k}}^{n\tau}$ and wave function $\phi_{\mathbf{k}}^{n\tau}(\mathbf{r})$ for the n -th moiré band at \mathbf{k} and τ . The interacting model is then constructed under the moiré band basis. Because all valence band states are below the Fermi energy for the charge-neutral twisted homobilayer, it is more convenient to use the hole basis for hole doped system. We define the hole operator as $b_{\mathbf{k}n\tau} = c_{\mathbf{k}n\tau}^\dagger$, where

$c_{\mathbf{k}n\tau}^\dagger$ is the creation operator for the Bloch state $\phi_{\mathbf{k}}^{n\tau}(r)$. The single-particle Hamiltonian $\hat{\mathcal{H}}_0$ in the hole basis can be written as

$$\hat{\mathcal{H}}_0 = \sum_{\mathbf{k}, \tau, n} \mathcal{E}_{\mathbf{k}}^{n\tau} b_{\mathbf{k}n\tau}^\dagger b_{\mathbf{k}n\tau}, \quad (\text{S13})$$

where $\mathcal{E}_{\mathbf{k}}^{n\tau} = -\varepsilon_{\mathbf{k}}^{n\tau}$ is the energy of Bloch state. In the hole representation, the Coulomb interaction projected onto the moiré bands is expressed as

$$\hat{\mathcal{H}}_{\text{int}} = \frac{1}{2} \sum V_{\mathbf{k}_1 \mathbf{k}_2 \mathbf{k}_3 \mathbf{k}_4}^{n_1 n_2 n_3 n_4}(\tau, \tau') b_{\mathbf{k}_1 n_1 \tau}^\dagger b_{\mathbf{k}_2 n_2 \tau'}^\dagger b_{\mathbf{k}_3 n_3 \tau'} b_{\mathbf{k}_4 n_4 \tau}, \quad (\text{S14})$$

where the summation is over the momentum \mathbf{k}_j (summed over the moiré Brillouin zone), the moiré band index n_j , and the valley index τ . The Coulomb matrix element is given by,

$$V_{\mathbf{k}_1 \mathbf{k}_2 \mathbf{k}_3 \mathbf{k}_4}^{n_1 n_2 n_3 n_4}(\tau, \tau') = \frac{1}{\mathcal{A}} \sum_{\mathbf{q}} V_{\mathbf{q}} M_{\mathbf{k}_1 \mathbf{k}_4}^{n_1 n_4}(\tau, \mathbf{q}) M_{\mathbf{k}_2 \mathbf{k}_3}^{n_2 n_3}(\tau', -\mathbf{q}), \quad (\text{S15})$$

where \mathcal{A} is the system area. The structure factor $M_{\mathbf{k}_1 \mathbf{k}_4}^{n_1 n_4}(\tau, \mathbf{q})$ is

$$M_{\mathbf{k}_1 \mathbf{k}_4}^{n_1 n_4}(\tau, \mathbf{q}) = \sum_l \int d\mathbf{r} e^{i\mathbf{q} \cdot \mathbf{r}} [\tilde{\phi}_{\mathbf{k}_1 l}^{n_1 \tau}(\mathbf{r})]^* \tilde{\phi}_{\mathbf{k}_4 l}^{n_4 \tau}(\mathbf{r}), \quad (\text{S16})$$

where $\tilde{\phi}_{\mathbf{k}}^{n\tau}(r) = [\phi_{\mathbf{k}}^{n\tau}(r)]^*$ due to the particle-hole transformation and l is the layer index. We use the dual-gate screened Coulomb interaction with the momentum-dependent potential $V_{\mathbf{q}} = 2\pi e^2 \tanh(|\mathbf{q}|d)/(\epsilon|\mathbf{q}|)$, where d is the gate-to-sample distance and ϵ is the dielectric constant. In our calculation, we set $d = 20$ nm, $\epsilon = 20$.

The full Hamiltonian $\hat{\mathcal{H}}$ of the interacting system is,

$$\hat{\mathcal{H}} = \hat{\mathcal{H}}_0 + \hat{\mathcal{H}}_{\text{int}}. \quad (\text{S17})$$

C. Mean-field Calculation

Based on Hartree-Fock approximation of $\hat{\mathcal{H}}_{\text{int}}$, we perform self-consistent calculations to study the ground states of $\hat{\mathcal{H}}$ for integer filling factors $\nu = 1$ at zero temperature. Here $\nu = \frac{1}{N_k} \sum_{\mathbf{k}, n, \tau} b_{\mathbf{k}n\tau}^\dagger b_{\mathbf{k}n\tau}$ is the number of holes per moiré unit cell, and N_k is the number of \mathbf{k} points in the summation. Starting from various symmetry-broken mean-field ansatzes, we self-consistently generate different mean-field solutions and compare their energy to determine the mean-field ground state. We calculate the phase diagram as a function of the twist angle θ , with the gate-to-sample distance d and the dielectric constant ϵ fixed. The parameter d can be controlled by the thickness of the encapsulating hBN layer. The dielectric constant ϵ accounts for the environmental screening from hBN as well as internal screening from remote moiré bands. Here we take ϵ as a phenomenological parameter.

III. CALCULATION OF OPTICAL MATRIX ELEMENT

The velocity operator \hat{v} can be expressed as follows,

$$\begin{aligned} \hat{v} &= \sum_{\mathbf{k}, \tau} \sum_{mn} \mathbf{J}_{mn}^\tau(\mathbf{k}) c_{\mathbf{k}m\tau}^\dagger c_{\mathbf{k}n\tau} = - \sum_{\mathbf{k}, \tau} \sum_{mn} [\mathbf{J}_{mn}^\tau(\mathbf{k})]^* b_{\mathbf{k}m\tau}^\dagger b_{\mathbf{k}n\tau} = \sum_{\mathbf{k}, \tau} \sum_{\lambda\lambda'} \mathbf{v}_{\tau, \lambda\lambda'}(\mathbf{k}) f_{\mathbf{k}\lambda\tau}^\dagger f_{\mathbf{k}\lambda'\tau}, \\ \mathbf{J}_{mn}^\tau(\mathbf{k}) &= \langle \phi_{\mathbf{k}}^{m\tau} | \frac{\partial \hat{\mathcal{H}}_0^\tau}{\partial \hat{\mathbf{k}}} | \phi_{\mathbf{k}}^{n\tau} \rangle, \\ \mathbf{v}_{\tau, \lambda\lambda'}(\mathbf{k}) &= - [U_{m\lambda}^{k\tau}]^* [\mathbf{J}_{mn}^\tau(\mathbf{k})]^* U_{n\lambda'}^{k\tau}, \end{aligned} \quad (\text{S18})$$

where $f_{\mathbf{k}\lambda\tau}^\dagger (f_{\mathbf{k}\lambda\tau})$ is the creation (annihilation) operator of Hartree-Fock quasiparticles of the λ -th band at \mathbf{k} of valley τ . Here $f_{\mathbf{k}\lambda\tau}^\dagger$ and $b_{\mathbf{k}n\tau}^\dagger$ operators are related by unitary transformations, $f_{\mathbf{k}\lambda\tau}^\dagger = \sum_n U_{n\lambda}^{k\tau} b_{\mathbf{k}n\tau}^\dagger$. According to Eq. (S12), $\frac{\partial \hat{\mathcal{H}}_0^\tau}{\partial \hat{\mathbf{k}}}$ can be expressed as,

$$\frac{\partial \hat{\mathcal{H}}_0^\tau}{\partial \hat{\mathbf{k}}} = \begin{pmatrix} -\frac{\hbar^2(\hat{\mathbf{k}} - \tau \boldsymbol{\kappa}_+)}{m^*} & 0 \\ 0 & -\frac{\hbar^2(\hat{\mathbf{k}} - \tau \boldsymbol{\kappa}_-)}{m^*} \end{pmatrix}. \quad (\text{S19})$$

Using Eq. (S18) and the exciton wave function of Eq. (10) in the main text, we derive the optical matrix element as,

$$V_{\chi G} = \langle \chi | \hat{v}_+ | G \rangle = \sum_{\mathbf{k}', \lambda'' \geq 2} \sum_{\mathbf{k}, \lambda \lambda'} [z_{\mathbf{k}', \lambda''}(\chi)]^* \mathbf{v}_{+, \lambda \lambda'}(\mathbf{k}) \langle G | f_{\mathbf{k}'1+}^\dagger f_{\mathbf{k}'\lambda''} + f_{\mathbf{k}\lambda+}^\dagger f_{\mathbf{k}\lambda'+} | G \rangle = \sum_{\mathbf{k}, \lambda \geq 2} [z_{\mathbf{k}, \lambda}(\chi)]^* \mathbf{v}_{+, \lambda 1}(\mathbf{k}). \quad (\text{S20})$$

Equation (S20) is used in the calculation of the optical conductivity.

IV. DERIVATION OF f SUM RULE

Here, we also give the derivation of the f sum rule presented in Eq. (12) in the main text. According to Eq. (S1), we obtain

$$W_{\alpha\alpha}^{(0)} = \int_0^\infty d\omega \text{Re}\sigma_{\alpha\alpha}(\omega) = \frac{e^2}{\hbar} \frac{\pi}{\mathcal{A}} \sum_{\chi} w_{\alpha\alpha}^{(0)}(\chi), \quad (\text{S21})$$

where $w_{\alpha\alpha}^{(0)}(\chi) = V_{G\chi}^\alpha V_{\chi G}^\alpha / \mathcal{E}_\chi$. By incorporating $\hat{v} = i[\hat{\mathcal{H}}, \hat{r}]$ into $V_{G\chi}^\alpha = \langle G | \hat{v}^\alpha | \chi \rangle$ and $V_{\chi G}^\alpha = \langle \chi | \hat{v}^\alpha | G \rangle$,

$$\begin{aligned} \sum_{\chi} w_{\alpha\alpha}^{(0)}(\chi) &= \frac{i}{2} \sum_{\chi} \frac{\langle G | \hat{\mathcal{H}} \hat{r}^\alpha - \hat{r}^\alpha \hat{\mathcal{H}} | \chi \rangle \langle \chi | \hat{v}^\alpha | G \rangle}{\mathcal{E}_\chi} + \frac{i}{2} \sum_{\chi} \frac{\langle G | \hat{v}^\alpha | \chi \rangle \langle \chi | \hat{\mathcal{H}} \hat{r}^\alpha - \hat{r}^\alpha \hat{\mathcal{H}} | G \rangle}{\mathcal{E}_\chi} \\ &= -\frac{i}{2} \sum_{\chi} \langle G | \hat{r}^\alpha | \chi \rangle \langle \chi | \hat{v}^\alpha | G \rangle + \frac{i}{2} \sum_{\chi} \langle G | \hat{v}^\alpha | \chi \rangle \langle \chi | \hat{r}^\alpha | G \rangle \\ &= -\frac{i}{2} \langle G | [\hat{r}^\alpha, \hat{v}^\alpha] | G \rangle = \frac{\hbar N_c}{2m^*}, \end{aligned} \quad (\text{S22})$$

where N_c is the total number of carriers. Then Eq. (S21) can be written as

$$W_{\alpha\alpha}^{(0)} = \int_0^\infty d\omega \text{Re}\sigma_{\alpha\alpha} = \frac{\pi n_c e^2}{2m^*}. \quad (\text{S23})$$

The charge density n_c at $\nu = 1$ is $1/\mathcal{A}_0$, where $\mathcal{A}_0 = \frac{\sqrt{3}}{2} a_M^2$ is the area of moiré unit cell.

V. REAL-SPACE EXCITON WAVEFUNCTION

The exciton state in momentum-space is parametrized as,

$$|\chi\rangle = \sum_{\mathbf{k}, \lambda \geq 2} z_{\mathbf{k}, \lambda}(\chi) f_{\mathbf{k}\lambda+}^\dagger f_{\mathbf{k}1+} | G \rangle. \quad (\text{S1})$$

We expand $f_{\mathbf{k}\lambda+}^\dagger$ ($f_{\mathbf{k}1+}$) by field operators at real space position \mathbf{r} in layer l as

$$f_{\mathbf{k}\lambda+}^\dagger = \sum_l \int d\mathbf{r} \psi_{\mathbf{k}l}^{\lambda+}(\mathbf{r}) f_{l\mathbf{r}}^\dagger, \quad f_{\mathbf{k}1+} = \sum_l \int d\mathbf{r} [\psi_{\mathbf{k}l}^{1+}(\mathbf{r})]^* f_{l\mathbf{r}}. \quad (\text{S2})$$

Then Eq. (S1) can be written as

$$|\chi\rangle = \sum_{l, l'} \int d\mathbf{r} \int d\mathbf{r}' g_{ll'}^\chi(\mathbf{r}, \mathbf{r}') f_{l\mathbf{r}}^\dagger f_{l'\mathbf{r}'} | G \rangle, \quad (\text{S3})$$

where $g_{ll'}^\chi(\mathbf{r}, \mathbf{r}') = \sum_{\mathbf{k}, \lambda \geq 2} z_{\mathbf{k}, \lambda}(\chi) \psi_{\mathbf{k}l}^{\lambda+}(\mathbf{r}) [\psi_{\mathbf{k}l'}^{1+}(\mathbf{r}')]^*$ is the real space exciton wavefunction. Here $\psi_{\mathbf{k}l}^{\lambda+}(\mathbf{r})$ ($\psi_{\mathbf{k}l}^{1+}(\mathbf{r})$) is the quasiparticle Bloch wavefunction at valley $\tau = +$ obtained by the mean-field calculation.

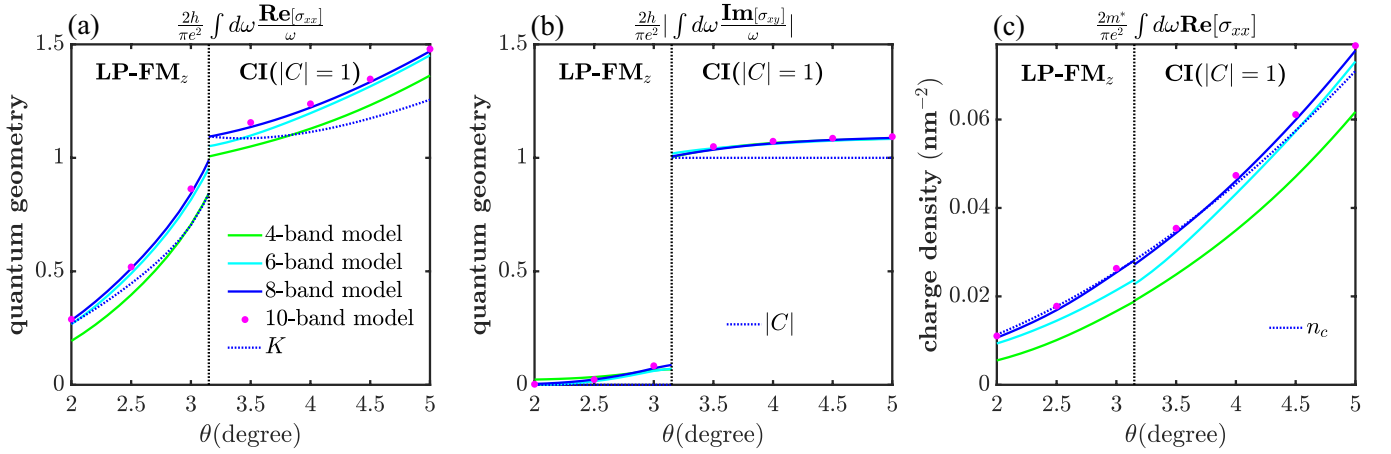


FIG. S1. Numerical results of optical sum rules calculated by including different numbers of moiré valence bands. (a), (b) The generalized optical weight $W_{\alpha\beta}^{(1)}$ with its real part in (a) and imaginary part in (b). (c) The optical spectral weight $W_{\alpha\beta}^{(0)}$. The results in (a), (b) and (c) are compared with quantum weight K (calculated using 8 moiré bands), Chern number $|C|$, and charge density n_c , respectively. We use 24×24 k -mesh in the calculation.

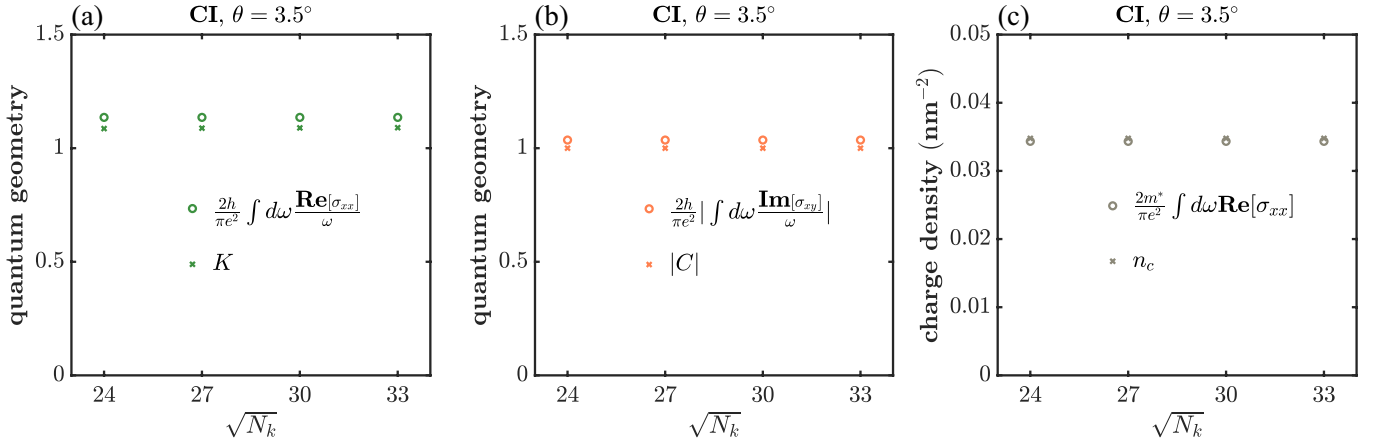


FIG. S2. Numerical results of optical sum rules for CI phase at $\theta = 3.5^\circ$ calculated using different sizes of k -mesh. (a), (b) The generalized optical weight $W_{\alpha\beta}^{(1)}$ with its real part in (a) and imaginary part in (b). (c) The optical spectral weight $W_{\alpha\alpha}^{(0)}$. The results in (a), (b), and (c) are compared with quantum weight K , Chern number $|C|$, and charge density n_c , respectively. We keep 8 moiré bands in the calculation.

VI. NUMERICAL CONVERGENCE

In principle, the sum rules should include excited states over all energies. However, as shown in Fig. 3 (a) in our main text, contributions from excited states with high energies can be ignored. This implies that the band-projected interacting model of Eq. (S14) can be truncated by including only a finite number of moiré bands. In Figs. S1, we compare the numerical results of both $W_{\alpha\beta}^{(1)}$ and $W_{\alpha\alpha}^{(0)}$ calculated by including different numbers of bands. We find that numerical convergence is reached by including 8 moiré bands.

We also compare the numerical results calculated using different sizes of k -mesh, as shown in Figs. S2. We find that $N_k = 24 \times 24$ is enough for numerical convergence.